Mode extraction technique for guided waves in a pipe

Takahiro Hayashi *, Morimasa Murase

Faculty of Engineering, Nagoya Institute of Technology

Gokiso Showa Nagoya, 466-8555, Japan

* Corresponding author (E-mail: hayashi@nitech.ac.jp)

Shortened running title: Guided wave mode extraction

Keywords:

guided wave, pipe inspection, mode extraction, normal mode expansion technique

Abstract

Guided waves propagating in a pipe consist of many modes with different velocities and dispersions. To analyze these complex guided waves through a normal mode expansion technique that is the fundamental theory on guided waves, we must first extract guided wave modes from received signals. In this study, we develop a mode extraction technique in which many received signals at different circumferential positions can be processed based on the fact that guided wave modes have different displacement distributions in the circumferential direction. After discussing the relevant theory, we verify our mode extraction technique experimentally using eight signals at eight different circumferential positions. Moreover, we show that the circumferential position of an excitation transducer, as well as the distance between an excitation transducer and a receiver in a pitch-catch configuration can be identified using the mode extraction technique.

INTRODUCTION

Acoustic signals can be detected dozens of meters away by applying vibration to the surface of pipes and elongated structures, such as railroad rails and I-beams, using impact hummers or ultrasonic transducers. This is possible because a group of acoustic energy waves propagates with no outward spreading, unlike bulk waves. Called “guided waves,” these acoustic waves have attracted attention recently as a means for rapid, nondestructive evaluation (NDE) of large structures.

Subsequent to the theoretical studies published by Gazis[1], considerable research has been done on guided wave propagation within pipes. Since the 1990’s, as demand has grown for a practical and fast method of conducting pipe inspections, a number of intensive studies on guided-wave NDE[2]-[7] have been done based on the achievements in plate inspection with Lamb waves[8]-[10]. However, as these systems are used increasingly in an ever-wider range of applications such as inspection of buried or meandering pipes (with or without defects and branches), various problems associated with guided waves have become apparent. For example, guided waves become greatly distorted in elbow regions, making it very difficult to detect defects beyond elbows. And, because wave propagation in a pipe is very complex due to dispersion and its multimodal nature, various signal-processing techniques are required to understand it correctly. In many cases, defect resolution with guided waves is not sufficient to meet the practical demands of pipe inspection.

To solve these problems, detected signals must first of all be strictly verified against guided wave theory. However, detected signals normally consist of a superposition of many modes having different velocities and dispersion characteristics. And a guided wave in a pipe, made up of modes with different displacement distributions in both the circumferential and thickness directions, has a more complex wave propagation than does a Lamb wave.

In this study, the authors develop a mode extraction technique for guided waves in a pipe. We first present a theoretical explanation of the technique. We then verify the theory experimentally for eight signals at eight different circumferential positions. In addition, the circumferential position of an excitation transducer, as well as the distance between an excitation transducer and a receiver, is determined using the mode extraction technique.

NORMAL MODE EXPANSION TECHNIQUE, DISPERSION CURVES AND WAVE STRUCTURES OF GUIDED WAVES

Before describing the mode extraction technique developed in this study, theories necessary for modal analysis of guided waves are briefly described. According to the normal mode expansion technique[1], [2], [11], [12] or semi-analytical finite element method[13], displacement at any of the points (r, θ, z) can be expressed using the orthogonal functions $\exp(in\theta)$ and $\exp(ik_{nm}z)$ for a harmonic wave $\exp(-i\omega t)$ as

$$u(r,\theta,z,t) = \sum_{n=-\infty}^{+\infty}\sum_{m=1}^{+\infty}\alpha_{nm}N_{nm}(r)\exp(in\theta + ik_{nm}z - i\omega t)\,, \qquad (1)$$

where integer n denotes the circumferential order, and k_{nm}, $N_{nm}(r)$ and α_{nm} are the wave number, function of the displacement distribution in the thickness direction and amplitude for the mth mode in the nth family, respectively. Similar to a Lamb wave, as mode number m increases, displacement distribution in the thickness direction $N_{nm}(r)$ becomes more complicated, and the resonant wave number k_{nm} has smaller real or complex values and a larger imaginary part. The complex wave number indicates a non-propagating mode that does not affect waveforms at receiving points sufficiently far from the source or reflective object. Therefore, the summation of an infinite number of m in Eq. (1) approximates to the summation of the first few propagating modes.

In Eq. (1) the term $\exp(in\theta)$, a function with circumferential order n, denotes a displacement distribution in the circumferential direction of the nth family. Here, n=0 means a uniform distribution in the circumferential direction, and n=+1 represents the distribution shown in Fig. 1 having maximum and minimum displacements on opposite sides of a pipe cross-section and zero displacements at 90° from the maximum and minimum points. In Fig. 1, bold arrows and thin arrows indicate the displacements in the plus and minus directions, respectively. The modes with n=0 and $n \neq 0$ are generally called axisymmetric and non-axisymmetric modes. The distribution of non-axisymmetric modes changes with time, as shown schematically in Fig. 2, where the displacement distribution is represented by bold lines at standard time ωt=0, and by solid, dashed and dotted lines at ωt=π/2, π and 3π/2, respectively. In the figure, n=-1 indicates rotation opposite to n=+1 (-θ direction). Similarly, Fig. 2(b) shows the displacement distributions for n=+2 and -2. As the absolute value of n increases, the displacement distribution in the circumferential direction becomes complex, and positive and negative circumferential orders indicate +θ and -θ rotations of displacement distribution, respectively.

FIG.1

FIG.2

An infinite number of resonant wave numbers k_{nm} ($m = 1,2\ldots+\infty$) can be obtained from the resonant condition for a circumferential order n. Some wave numbers k_{nm} are real values that imply propagating modes, and other k_{nm} are complex values that imply non-propagating modes. Normally, only propagating modes are used in guided-wave

NDE. After calculating the wave numbers, we can obtain phase velocities from $c_{nm} = \omega / k_{nm}$ and group velocities from the slope of phase velocities. Then, phase and group velocity dispersion curves are obtained by plotting solutions at each frequency step (Fig. 3). The dispersion curves give fundamental information for guided-wave NDE[13]. These curves are conventionally denoted by T(n,m), L(0,m) and F(n,m). The n and m within parentheses correspond to the circumferential order n and the mode number m, respectively, in Eq. (1). It should be noted, however, that different nomenclature may be adopted in other literature for the modes of guided waves. In this paper, we use the notation from a detailed discussion on the subject by Nishino et al[14]. . Since modes of plus and minus n are symmetrical with respect to the pipe axis, they have the same phase and group velocities. Although these modes with plus and minus n have generally been considered the same mode, we regard them as different modes for a strictly theoretical treatment and refer to them as the +nth and –nth circumferential modes.

FIG.3

THEORY OF CIRCUMFERENTIAL MODE EXTRACTION

Axisymmetric modes with the same phase in the circumferential direction can be extracted by summing up signals in receiving sensors located in the circumferential direction at regular intervals. Other modes with non-uniform phases varying in the circumferential direction become zero in the resulting signals. This is due to the orthogonality of exp$(in\theta)$. Similarly, non-axisymmetric modes can be extracted by using the orthogonality of exp$(in\theta)$.

For example, let us consider mode extraction for n=+1, which moves with the displacement distribution shown in Fig. 2 (a). We assume that receiving sensors are located at the four circumferential positions (upper, lower, right and left sides) in Fig. 2. Since the component of an n=+1 mode in signals detected at the right and left sides have opposite phases, their difference yields large signals of the n=+1 mode. Similarly, the difference of signals at the upper and lower positions yield large signals of the n=+1 mode. Thus, non-axisymmetric modes can be extracted by summing up the signals detected at many circumferential positions having the appropriate weight functions. However, since other unwanted modes may be superposed in these signals, a more detailed theoretical basis for the mode extraction technique is required for further modal analysis. This sention describes a mode extraction theory that uses the orthogonality of exponential functions.

From Eq. (1), a complex displacement at an arbitrary circumferential position θ can be expressed by the complex amplitude of nth circumferential order A_n and orthogonal function $\exp(in\theta)$ as

$$u(\theta) = \sum_{n=-\infty}^{+\infty} A_n \exp(in\theta) . \tag{2}$$

Received signals at a small region of $r_0 d\theta$ on the outer surface of a pipe (outer diameter = $2r_0$) are given by

$$du = \sum_{n=-\infty}^{+\infty} A_n \exp(in\theta) r_0 d\theta . \tag{3}$$

Multiplying $\exp(-in_E\theta)$ as a weight function in Eq. (3), and then integrating this with respect to θ, gives the waveforms

$$u^{ext}{}_{n_E} = \int_0^{2\pi} \sum_{n=-\infty}^{+\infty} A_n \exp\{i(n-n_E)\theta\} r_0 d\theta = 2\pi r_0 A_{n_E} . \tag{4}$$

That is, if an infinite number of infinitesimal sensors are placed on the surface of a pipe, the summation of these waveforms with weight function $\exp(-in_E\theta)$ gives extracted waveforms of the n_Eth circumferential mode.

In actual situations, receiving sensors are not infinitesimal as $r_0 d\theta$, and the number of receiving points is also finite. Assuming N receiving positions in the circumferential direction at regular intervals as

$$\theta_k = \frac{2\pi}{N}(k-1), \tag{5}$$

and a displacement is detected in the region with an aperture of $\theta_0 = 2\pi/N$, then the received signals at $\theta = \theta_k$ and $z = z_R$ are

$$u^R(\theta_k, z_R, t) = \int_{\theta_k-\theta_0/2}^{\theta_k+\theta_0/2} u(\theta, z_R, t) r_0 d\theta$$

$$= r_0 \sum_{n=-\infty}^{+\infty} \alpha_n f_n(\theta_0) \exp(in\theta_k + ik_n z_R - i\omega t), \tag{6}$$

where

$$f_n(\theta_0) = \begin{cases} \theta_0 & for \quad n = 0 \\ \dfrac{2\sin(n\theta_0/2)}{n} & for \quad n \neq 0 \end{cases}. \tag{7}$$

FIG.4

Here, $f_n(\theta_0)$ has a constant value θ_0 for n=0, and varies with the aperture of sensors θ_0 for $n \neq 0$. Fig. 4 shows $f_n(\theta_0)/\theta_0$ versus n for five representative apertures of sensors θ_0. For all apertures θ_0, the maximum value of $f_n(\theta_0)/\theta_0$ is 1.00 at n=0. When satisfying $\sin n\theta_0/2 = 0$, that is,

$$\theta_0 = \frac{2l}{n}\pi \qquad l = 1,2,3\ldots n, \tag{8}$$

then $f_n(\theta_0)$ becomes zero. An axisymmetric mode with a circumferential order of zero is always detected at receiving sensors of any aperture, while non-axisymmetric modes with $n \neq 0$ may not be superposed in detected signals. Generally speaking, those receiving sensors with smaller apertures can detect higher *n*th order modes.

Similarly to Eq. (4), multiplying weight function $\exp(-in_E\theta_k)$ and summing with respect to *k* gives

$$u^{ext}{}_{n_E}(t) = r_0 \sum_{k=1}^{N} \sum_{n=-\infty}^{+\infty} \alpha_n f_n(\theta_0) \exp(in\theta_k + ik_n z_R - i\omega t) \exp(-in_E\theta_k)]$$

$$= r_0 \sum_{n=-\infty}^{+\infty} \left[\alpha_n f_n(\theta_0) \exp(ik_n z_R - i\omega t) \sum_{k=1}^{N} \exp\{i(n-n_E)\theta_k\} \right] \qquad (9)$$

where

$$\sum_{k=1}^{N} \exp\{i(n-n_E)\theta_k\} = \begin{cases} 0 & at \quad n \neq n_E \pm Nl \\ N & at \quad n = n_E \pm Nl \end{cases} \qquad l = 0, \pm 1, \pm 2, \pm 3 \ldots$$

$$(10)$$

These equations indicate that the modes with circumferential order $n = n_E \pm Nl$ are superposed in the resulting waveforms $u^{ext}{}_{n_E}$ together with target mode n=n_E. For example, let us consider the case in which there are eight receiving positions (N=8). For extraction target modes $n_E = 0, \pm 1, \pm 2, \pm 3$, the unwanted detectable modes are higher order than the target n_E. But for $n_E = \pm 4$, modes with the opposite sign $n=\mp 4$ are included in the extracted signals, and for $n_E = \pm 5$, the lower mode of n=-3 can be detected.

Usually, higher order modes are small in received signals due to strong dispersion and cutoff frequencies. Also, function $f_n(\theta_0)$ acts to lessen the higher order modes.

Therefore, it can be concluded that this mode extraction technique is useful for $|n_E| \leq N/2-1$, and Eq. (9) can be rewritten, under the condition of $|n_E| \leq N/2-1$, as the approximation

$$u^{ext}{}_{n_E}(t) \approx r_0 \alpha_{n_E} f_{n_E}(\theta_0) \exp(ik_{n_E} z_R - i\omega t). \tag{11}$$

EXPERIMENT

Mode extraction tests are conducted for an aluminum pipe with an outer diameter of 111 mm and thickness of 3.5 mm. The dispersion curves for the pipe are shown in Fig. 3. EMATs are used to excite and receive ultrasonic energy in a pitch-catch configuration. Two EMATs are located one meter in from either pipe end and two meters apart from one another, as shown in Fig. 5. An excitation EMAT is fixed at a circumferential position of 0° using two different skew angles of 0° and –45°. A receiving EMAT is placed at eight different circumferential positions (0°, 45°, 90°, 135°, 180°, 225°, 270°, 335°), in turn. The EMATs consist of two permanent magnets (NEOMAX, NEOMAT Co. Ltd., 15 mm x 6 mm x 10 mm) and sheet coils fabricated by a printed-circuit technique. The EMATs are flexible to fit the curvature of the pipe. The sheet coil and permanent magnets of the EMATs are arranged to excite and receive shear horizontal waves by Lorents forces. These transducers, then, generate and receive vibration mainly in the circumferential direction[15]. The active width of the EMATs in the circumferential direction is one eighth of the circumference. A two-channel signal generator (NF corporation, WF1944A) generates 50-kHz, 4-cycle tone-burst waves, which are then magnified to 32 dB by power amplifiers (NF corporation, HSA4051). The received signals are amplified 40 dB by a preamplifier and recorded after 10 signal averagings.

FIG.5

Fig. 6 shows signals detected at eight different circumferential positions using an excitation EMAT at a skew angle of 0º. These signals give no information whatsoever on guided wave modes. Fig. 7 shows the waveforms extracted from the signals of Fig. 6 using Eq. (9). Because Eq.(9) treats measured signals as complex values, this equation cannot, in fact, be applied directly to real measured signals.

FIG.6

FIG.7

Multiplying the measured signals with real values $u^{meas}{}_k$ (k=1,..,N) by $\exp(-in_E\theta_k)$ and summing gives the following waveforms.

$$u^{ext,meas} = \sum_{k=1}^{N} u^{meas}{}_k \exp(-in_E\theta)$$

$$\begin{aligned} &= \sum_{k=1}^{N} u^{meas}{}_k \cos(-n_E\theta) + i\sum_{k=1}^{N} u^{meas}{}_k \sin(-n_E\theta) \\ &= \sum_{k=1}^{N} u^{meas}{}_k \frac{e^{-in_E\theta} + e^{in_E\theta}}{2} + i\sum_{k=1}^{N} u^{meas}{}_k \frac{e^{-in_E\theta} - e^{in_E\theta}}{2i} \end{aligned} \tag{12}$$

Waveforms $u^{ext,meas}$, obtained through a mode extraction process applied to real measured signals, yields complex waveforms. In Eq. (12), the real part of $u^{ext,meas}$ means the sum of the extracted waveforms of n=+n_E and n=-n_E, and the imaginary part shows the difference between the extracted waveforms of n=+n_E and n=-n_E. The imaginary unit i indicates a phase shift of π/2. Thus, the sum of the real part of Eq. (12), and the waveforms of the imaginary part, phase–shifted by π/2, results in the extracted waveforms of n=+n_E (which were shown in Fig. 7). To shift the phase back by π/2 in the imaginary part, the waveforms of the imaginary part are advanced T/4 in time, where T is the period of the center frequency 50 kHz (31.25 μs).

In Fig. 7, large waveforms are obtained at the moment corresponding to the group velocities of the target circumferential orders, respectively. In $n_E = \pm 2$, F($\pm$2,2) modes dominated by longitudinal vibration are detected together with shear horizontal modes T($\pm$2,1). F($\pm$2,2) appear about at 500-650μs, implying that the F($\pm$2,2) modes have larger group velocities than T($\pm$2,1) as seen in the dispersion curves of Fig. 3. Also, similar waveforms are obtained for the same absolute value of n_E. This is because the excitation EMAT emits ultrasonic energy symmetrically, and the amplitudes of plus and minus modes become the same.

Next, let us consider the case in which asymmetrical waves are excited in a pipe by skewing the excitation EMAT. The skew angle is –45°, as shown in Fig. 5. Fig. 8 shows the extracted waveforms for target modes n_E (n_E=-3 to +3). These signals have apparently different waveforms for $\pm$ signs, unlike those of Fig. 7. The T(-2,1) and T(-3,1) modes are larger than those of T(+2,1) and T(+3,1), respectively, indicating that waves rotating in the $-\theta$ direction are dominant. On the contrary, a waveform with a plus sign of flexural mode F(+2,2) is larger than one with a minus sign, showing that longitudinal waves largely propagate in the $+\theta$ direction due to skew of the EMAT.

FIG.8

IDENTIFICATION OF THE CIRCUMFERENCIAL POSITION OF A POINT SOURCE BY THE MODE EXTRACTION TECHNIQUE

The guided wave modes used in NDE are propagating modes that have real wave numbers. They can propagate above the cut-off frequency given for axisymmetric torsional modes T(0,m) as

$$f_c = \frac{c_T}{2d}(m-1) \tag{13}$$

where c_T is the transverse wave velocity and d is the thickness of the pipe. Considering torsional modes with $m \geq 2$, the cutoff frequency exceeds the 20-200 kHz frequency region generally used in guided-wave NDE. For example, the cutoff frequency of a T(0,2) mode for an aluminum pipe used in this study is $f_c = 440$ kHz. Therefore, we can assume that modes with m=1 can exist. Displacements on the pipe surface, as described in Eq. (1), can be rewritten by retaining the terms of m=1 as

$$u(\theta, z, t) = \sum_{n=-\infty}^{+\infty} \alpha_n \exp(in\theta + ik_n z - i\omega t). \tag{14}$$

Now, assuming that an excitation transducer is placed at $\theta=\theta_S$ and $z=z_S$, then the displacement at $z=z_S$ is expressed using a delta function as

$$u(\theta, z_S, t) = \frac{A}{2\pi}\delta(\theta - \theta_S)\exp(-i\omega t) \tag{15}$$

where A is an arbitrary constant. From Eqs. (14) and (15),

$$\sum_{n=-\infty}^{+\infty} \alpha_n \exp(in\theta + ik_n z_S) = \frac{A}{2\pi}\delta(\theta - \theta_S) \tag{16}$$

is obtained. Multiplying by $\exp(-in'\theta)$ in Eq. (16) and integrating with respect to θ gives

$$\alpha_{n'} = A\exp(-ik_{n'} z_S - in'\theta_S). \tag{17}$$

Using this relationship, displacement at an arbitrary point is given by rewriting Eq. (14) as,

$$u(\theta, z, t) = A\sum_{n=-\infty}^{+\infty} \exp\{in(\theta - \theta_S) + ik_n(z - z_S) - i\omega t\}. \tag{18}$$

As shown in the previous section, received signals for a transducer of aperture θ_0 at $\theta=\theta_k$ and $z=z_R$ are obtained by integrating with respect to θ as

$$u_R(\theta_k, z_R, t) = A\sum_{n=-\infty}^{+\infty} f_n(\theta_0)\exp\{in(\theta_k - \theta_S) + ik_n(z_R - z_S) - i\omega t\}. \tag{19}$$

Let us now consider the single mode extraction of a target mode n_E as in the previous section. Summing all u_R with weight function $\exp(-in_E\theta_k)$ gives the following approximated equation of an extracted waveform $n = n_E$:

$$u^{ext}{}_{n_E} \approx Af_{n_E}(\theta_0)\exp\{-in_E\theta_S + ik_{n_E}(z_R - z_S) - i\omega t\}. \tag{20}$$

Exact solutions are expressed as a summation with respect to n, but for a large number of receiving points N and small target mode number n_E, the waveforms of extraction target n_E can be approximated as Eq. (20).

In guided-wave NDE, the distance between a source and the receiving points has often been obtained by finding the arrival time of an extracted T(0,1) mode. Here, we consider finding the circumferential position θ_S. First, the phases of n_E=0 and n_E=+1 are compared. The time of maximum amplitudes are t_0 and t_{+1}, respectively. Since the phases at these moments are the same, the following equation is satisfied as

$$k_0(z_R - z_S) - \omega t_0 = -\theta_S + k_1(z_R - z_S) - \omega t_{+1} + 2\pi l \tag{21}$$

where l is an integer. Rearranging Eq. (21) gives

$$\theta_S = (k_1 - k_0)(z_R - z_S) - \omega(t_{+1} - t_0) + 2\pi l\,. \tag{22}$$

Here, $k_1 - k_0$ is calculated by theoretical dispersion curves, and $z_R - z_S$ is calculated by extracted waveforms of T(0,1) and group velocity of T(0,1). Also, $t_{+1} - t_0$ is obtained by the time difference between extracted waves of T(+1,1) and T(0,1). Substituting these values into Eq. (22) gives a circumferential position of the source θ_S.

For example, in the extracted waveforms of Fig. 7 (a zoomed-in view of these waveforms is shown in Fig. 9), $t_{+1} - t_0$=32.0[μs] and $z_R - z_S$=630[μs]x3080[m/s]=1.94[m], in which 630 [μs] is the arrival time of a T(0,1) mode. Then, theoretical dispersion curves *FIG.9* give $k_1 - k_0 \left[= \omega\left(\frac{1}{c_1} - \frac{1}{c_0}\right)\right]$ = -1.63[1/m] where c_1 and c_0 are the phase velocities of T(±1,1) and T(0,1) modes at 50 kHz. Substituting these values into Eq. (22) gives $\theta_S = -37^\circ$. Since the correct answer is 0°, it is clear that comparing the phases of T(0,1) and T(+1,1) does not yield a good answer. This is due to a large possible error in the term of $\frac{1}{c_1} - \frac{1}{c_0}$. The phase velocity of a non-dispersive T(0,1) mode can be easily determined as $c_0 = 3080$ [m/s], but the phase velocity of a dispersive T(+1,1) can only be determined with some error, about ± 20 m/s for example. If a T(+1,1) mode varies in the region of 3130 ± 20 m/s, then the resulting θ_S varies from –108° to 35°.

Therefore, let us consider a comparison of the phases of T(+1,1) and T(-1,1) modes. Assuming that t_{+1} and t_{-1} denote the time of maximum amplitude in the extracted T(+1,1) and T(-1,1) waveforms, respectively, then the phases at these moments are

$$-\theta_S + k_{+1}(z_R - z_S) - \omega t_{+1} = \theta_S + k_{-1}(z_R - z_S) - \omega t_{-1} - 2\pi l \qquad (23)$$

where l is an integer. Considering $k_1 = k_{+1} = k_{-1}$, Eq. (23) becomes

$$\theta_S = \omega\left(t_{-1} - t_{+1}\right) + \pi l \qquad (24)$$

which indicates that the circumferential position θ_S can be limited to two candidates. Since Eq. (24) does not contain wave number k_1, which may have large error, the circumferential position of a source θ_S can be determined more accurately than Eq. (23). In the case of Fig. 7, $t_{-1} - t_{+1} = -0.5$ μs gives the two candidates θ_S=-9°, 172°. One of these, –9°, is closer to the correct answer 0° than the –37° obtained using the phase difference between T(0,1) and T(+1,1) in Eq. (22).

When considering waves reflected from a defect, the defect can be regarded as an excitation point of various modes. Therefore, using the mode extraction technique, we can estimate the symmetry of the defect from plus and minus modes, and we can also determine the circumferential position of the defect by comparing phases in the extracted waveforms.

CONCLUSIONS

In this study, we developed a circumferential mode extraction technique necessary for characterizing defects using guided waves. We described the mode extraction technique theoretically as the separation of circumferential modes by detecting signals at many different circumferential positions and multiplying by the appropriate weight functions. Up to $\pm|N/2-1|$ circumferential order modes can be extracted using N signals detected at N different circumferential positions.

We verified the circumferential mode extraction theory experimentally using EMATs with pitch-catch testing. By skewing the excitation EMAT, the amplitudes of modes rotating in the plus and minus directions were found to differ indicating that asymmetrical guided waves were excited.

Two methods for identifying the circumferential position of a source were described. One uses the phase difference between T(0,1) and T(+1,1), and the other uses the phase difference between T(-1,1) and T(+1,1). The former method gives one circumferential position with large error, and the latter method gives two candidate circumferential positions with higher accuracy.

The mode extraction technique presented in this study can be used in defect characterization by applying the technique to reflected waves from a defect.

ACKNOWLEDGEMENTS

This research was supported by the Industrial Technology Research Grant Program in '03 from New Energy and Industrial Technology Development Organization (NEDO) of Japan. We thank Takashi Ikeda at the CXR Corporation for his considerable assistance with the magnetostrictive sensors.

References

1. D. C. Gazis, “Three-Dimensional Investigation of the Propagation of Waves in Hollow Circular Cylinders. I. Analytical Foundation and II Numerical Results,” J. Acoust. Soc. Am., **31** (5), 568-578 (1959)

2. J. J. Ditri and J. L. Rose, ” Excitation of guided elastic wave modes in hollow cylinders by applied surface tractions,” J. Appl. Phys. 72 (7), 2589-2597 (1992)

3. J. Li and J. L. Rose, “Excitation and propagation of non-axisymmetric guided waves in a hollow cylinder,” J. Acoust. Soc. Am., **109** (2), 457-468 (2001)

4. J. L. Rose, “Guided wave ultrasonic pipe inspection-The next generation”, Proceedings of the 8th ECNDT, Barcelona, Spain (2002)

5. D.N Alleyne and P. Cawley “Long range progagation of Lamb waves in chemical plant pipework,” Materials Evaluation, **55**, 504-508 (1997)

6. D. N. Alleyne, M. J. S. Lowe and P. Cawley, “The Reflection of Guided Waves From Circumferential Notches in Pipes,”J. Appl. Mech., **65**, 635-641 (1998)

7. P. Cawley, M. J. S. Lowe, D. N. Alleyne, B. Pavlakovic and P. Wilcox “Practical long range guided wave testing: Applications to pipes and rail,” Materials Evaluation, **61** (1), 66-74 (2003)

8. J. L. Rose, Ultrasonic waves in solid media, (Cambridge university press 1999)

9. P. Cawley and D. Alleyne, “The use of Lamb waves for the long range inspection of large structures,” Ultrasonics, **34**, 287-290, (1996)

10. P. Cawley and D. N. Alleyne, “The use of Lamb waves for the long range inspection of large structures,” Ultrasonics, **34**, 287-290 (1996)

11. G. S. Kino: Acoustic waves, Devices, imaging and digital signal processing (Prentice-Hall, Englewood Cliffs, NJ, 1987)

12. B. A. Auld, Acoustic fields and waves in solids (Krieger, Malabar, FL, 1990) Vol.II

13. T. Hayashi, W. Song and J. L. Rose, "Guided wave dispersion curves for a bar with an arbitrary cross-section, a rod and rail example," Ultrasonics, **41** (3), 175-183 (2003)

14. H. Nishino, S. Takashina, F. Uchida, M. Takemoto and K. Ono, "Modal analysis of hollow cylindrical guided waves and applications," Jpn. J. Appl. Phys. **40**, 364-370 (2001)

15. M. Hirao and H. Ogi, EMATs for science and industry – noncontacting ultrasonic measurements-, (Kluwer, 2003)

Figure Captions

FIG. 1. Displacement distribution for $n=\pm 1$ at ωt=0.

FIG. 2. Displacement distribution in the circumferential direction for the families of ± 1 and ± 2 at ωt=0, π/2, π, 3π/2.

FIG. 3. Group velocity dispersion curves for an aluminum pipe.

(Outer diameter=111.0mm, thickness=3.5mm, c_L=6260m/s, c_T=3080m/s)

FIG. 4. $f_n(\theta_0)/\theta_0$ versus circumferential order n for various widths of the sensor.

FIG. 5. EMATs and pipe arrangement.

An excitation EMAT is fixed at the circumferential position of 0^{o,} with two different skew angles of 0^{o} and –45^{o}. Received signals are detected at eight different circumferential positions with an EMAT.

FIG. 6 Received signals at eight different circumferential positions.

FIG. 7 Extracted waveforms from the signals shown in Fig. 6.

The incident wave is emitted in the pipe axis direction. n_E indicates the extraction target families.

FIG. 8 Extracted waveforms.

The incident wave is emitted at a skew angle of minus 45^{o} to the pipe axis. n_E indicates the extraction target families.

FIG. 9 Zoomed-in view of the waveforms in Fig. 7 for n_E=0 and ± 1

FIG.1

Hayashi

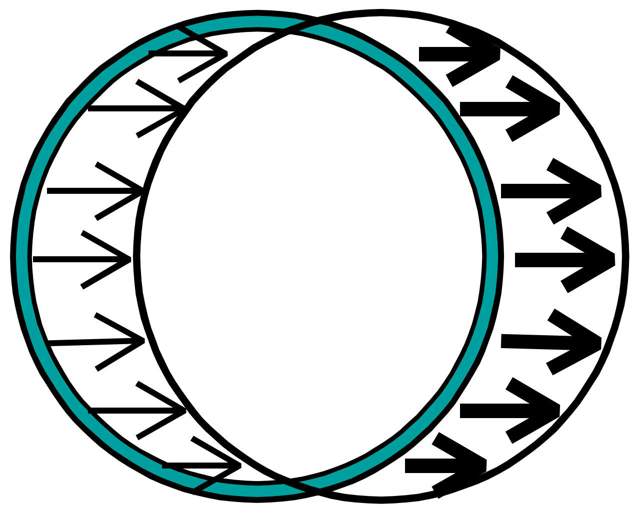

FIG.2

Hayashi

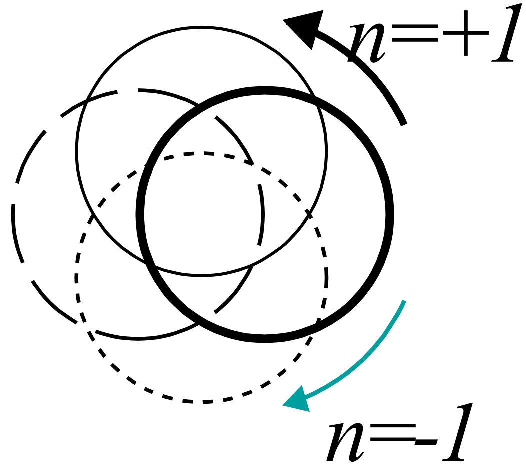

(a) $n = \pm 1$

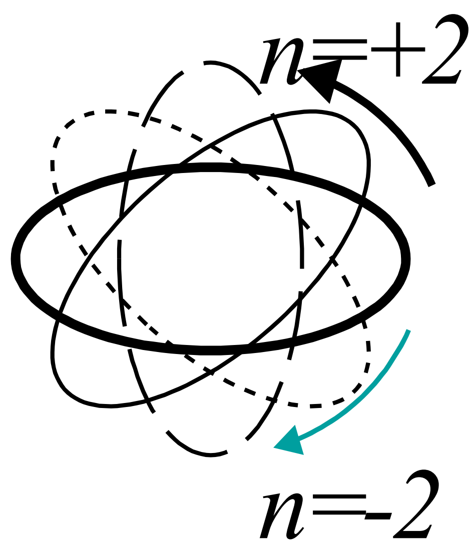

(b) $n = \pm 2$

FIG.3

Hayashi

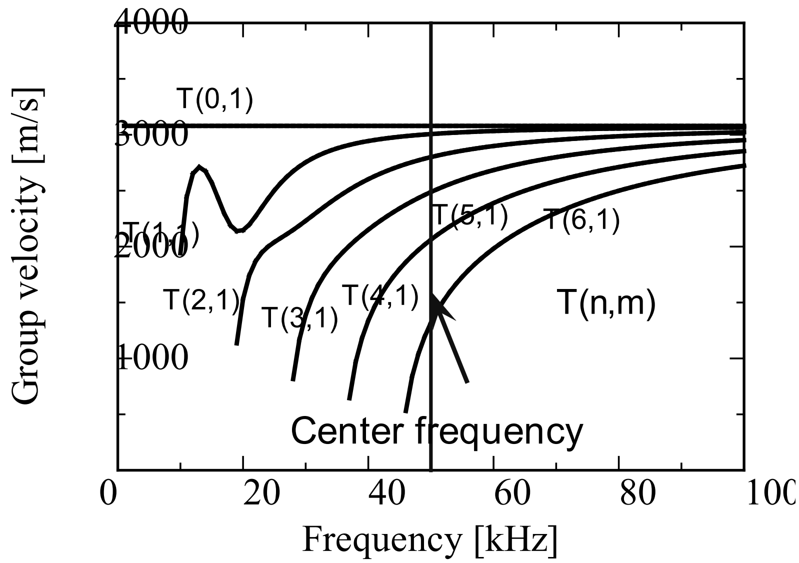

(a) Torsional modes

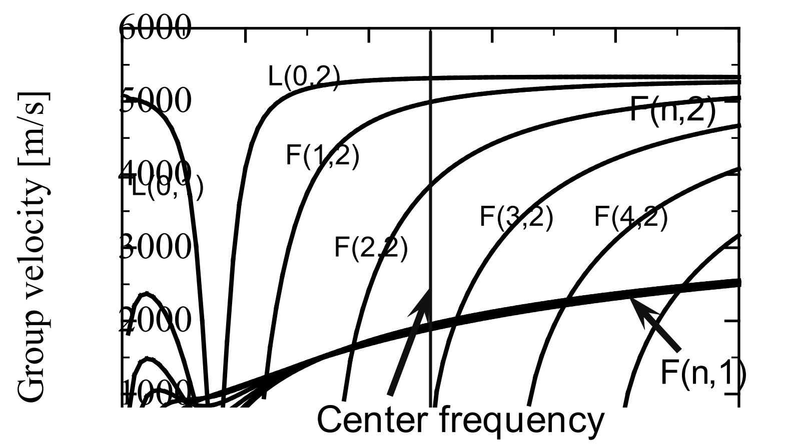

(b) Longitudinal and flexural modes

FIG.4

Hayashi

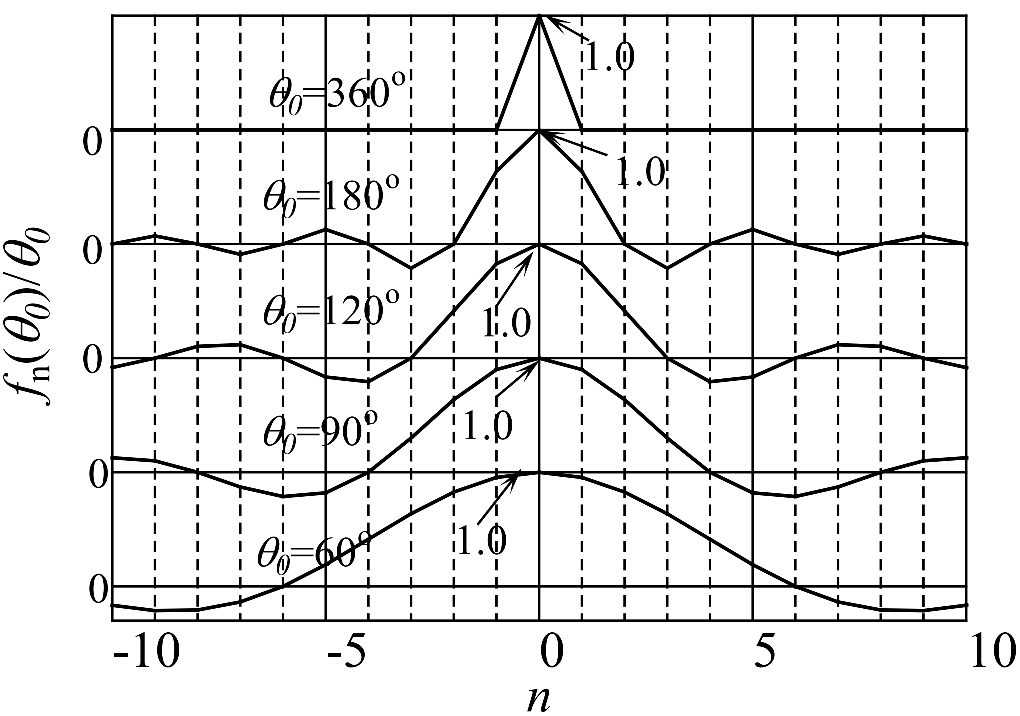

FIG.5

Hayashi

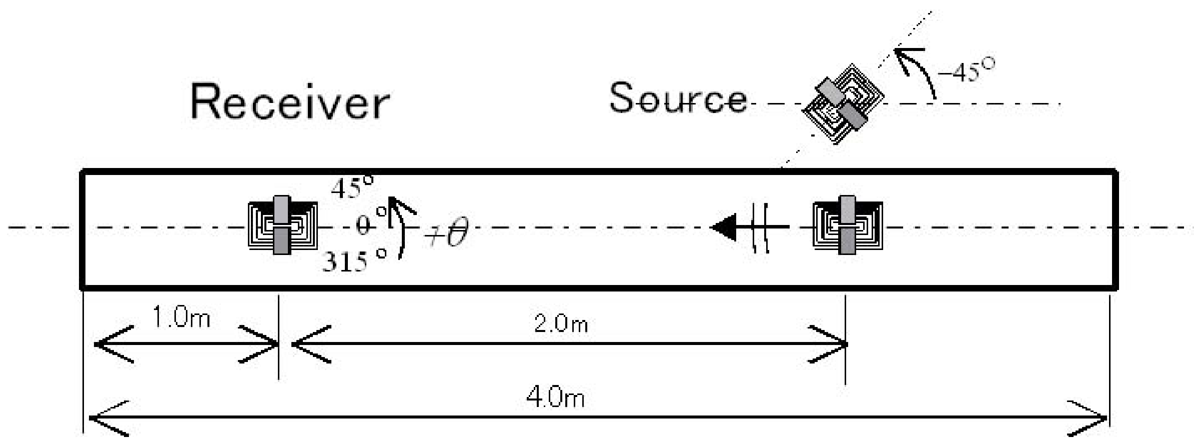

FIG.6

Hayashi

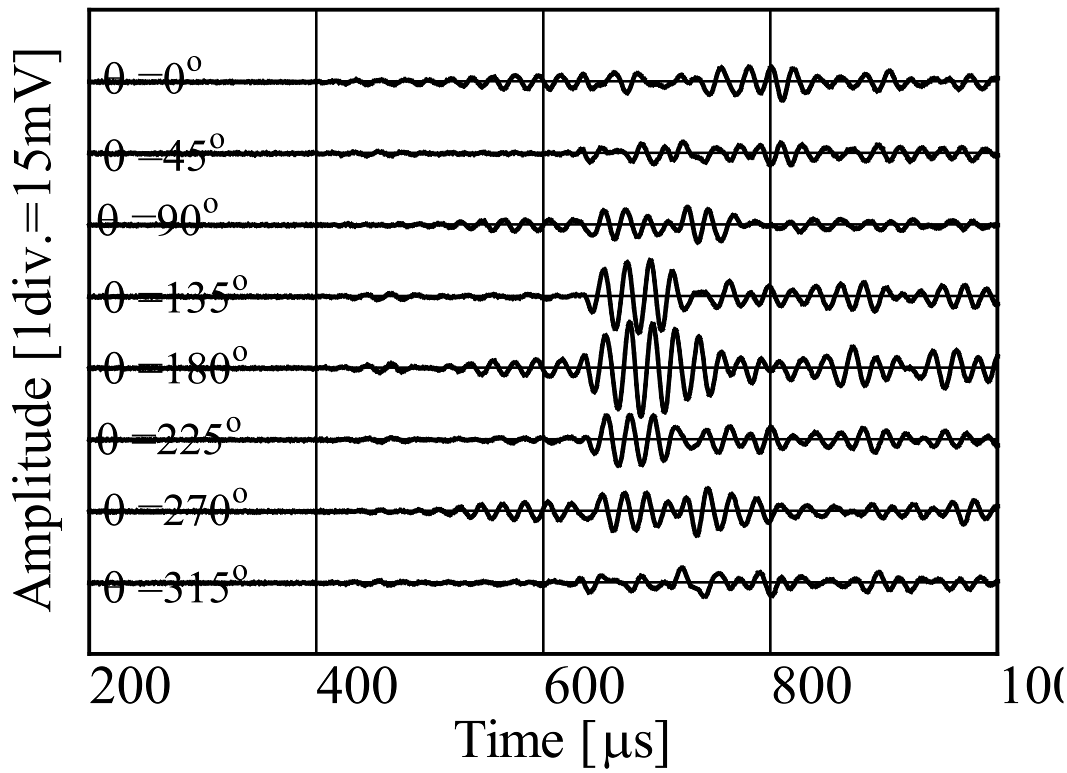

FIG.7

Hayashi

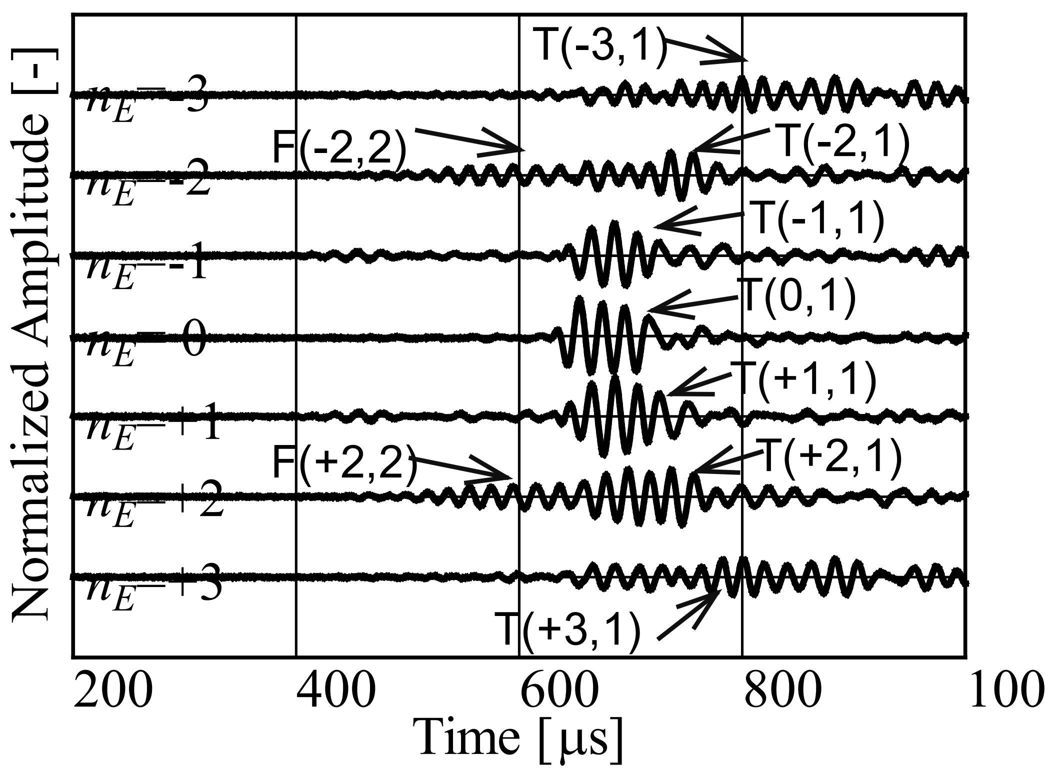

FIG.8

Hayashi

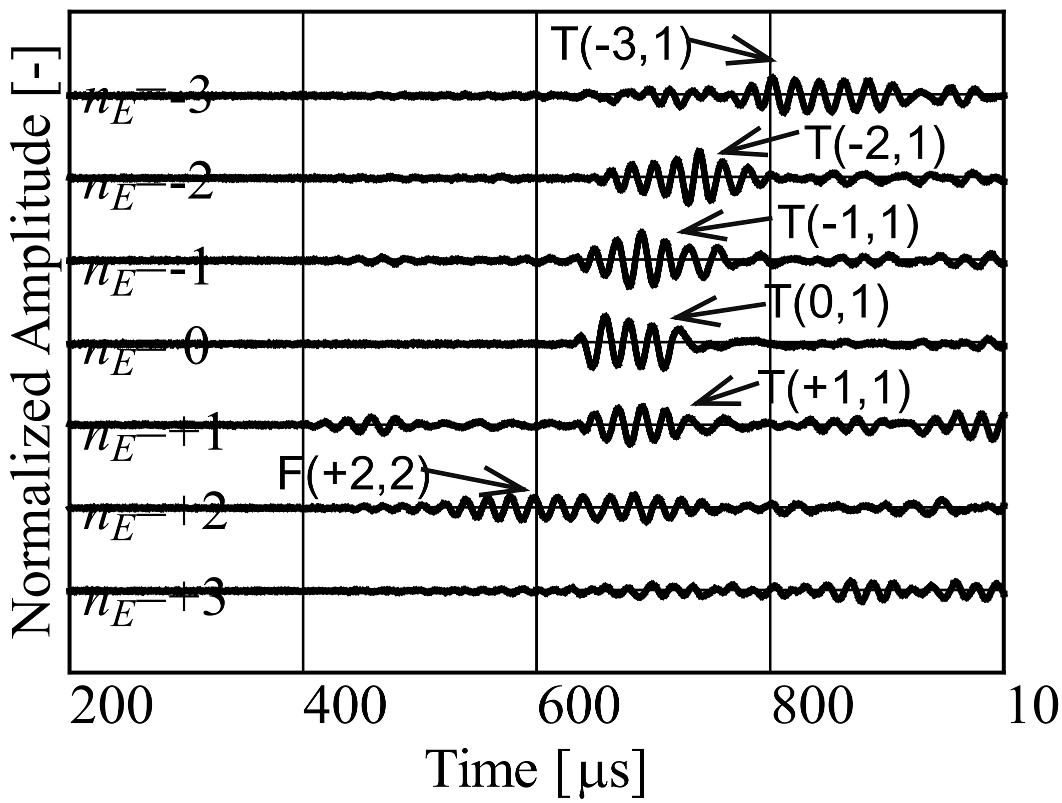

FIG.9

Hayashi